The effect of a cross-flow on secondary atomization in multipoint fuel injection systems

Diamantino F. Durão [1], António L. N. Moreira[2], Miguel R.O. Panão[3]

1: Universidade Lusíada, Portugal, durao@lis.ulusiada.pt
2: Dept. of Mechanical Engineering, Instituto Superior Técnico, Portugal, moreira@dem.ist.utl.pt
3: Dept. of Mechanical Engineering, Instituto Superior Técnico, Portugal, mpanao@dem.ist.utl.pt

Abstract The use of multipoint injection systems for HCCI engines requires a mixture composition precisely controlled in order to obtain the optimum auto-ignition timing. The most favorable injection timing to achieve it is when the intake valve is open, in which case the fuel spray interacts with the air flow and impacts onto interposed surfaces where it may form a liquid film, especially at engine cold-start, and eventually generate smaller droplets by mechanisms of secondary atomization. An accurate description of the physics of spray-wall impact under cross flow conditions and of the effects of the latter on secondary atomization are key issues to devise appropriate strategies to optimize the injection system and to control mixture preparation. This is the aim of the work reported here. The experiments consider overlapping of Mie and Shadowgraph visualization techniques and a phase-Doppler anemometer to visualize and quantify the effects of a cross-flow on spray impact and secondary droplets. Furthermore, the experiments were conducted for well-defined boundary conditions, thus providing results useful for the development spray/wall interaction models. Analysis show that: the cross-flow decelerates the axial velocity of impinging droplets, thus decreasing the energy available at impact; because drag is more efficient on those droplets more prone to adhere to the wall, the net effect is the formation of thinner films; this, in turn, enhances the generation of secondary drops which are then dragged away from re-impacting onto the wall.

1. Introduction

Shortcomings of the combustion process, as it occurs in internal combustion engines, has been evaluated and new combustion modes have recently been sought which raise new challenges to the design of appropriate fuel injection systems. In this context, a renewed interest is now arising on port fuel injection as a way to achieve homogeneous premixing for ultra lean combustion strategies, namely HCCI, where better production-cost to emissions ratios can be found (Milovanovic et al., 2005; Zhang et al., 2006). Port injection, in which the fuel is supplied from the upstream of inlet valves, allows optimization of exhaust, fuel consumption and engine output in addition to superiority in system cost by applying fuel atomization technology for continuous variation of the opening and closing timing, phase and lift of the inlet and exhaust valves, e g Cao et al. (2005). These authors also found that symmetric intake valve opening produces a more stratified mixture, earlier ignition timing, and localized combustion, i.e. a more favorable condition for HCCI, which means that the spray will interact with a cross-flow.

However, besides the interaction with the cross-flow, the quality of atomization and, therefore, mixture preparation and combustion depends on the thermal and fluid-dynamic interactions between fuel droplets, the valve and other interposed surfaces. In the case of dense sprays, such as those considered here, the outcome of impact is mostly influenced by multiple droplet interactions such as those between successive impacts, (e g Senda et al., 1988; Richter and Dullenkopf, 2005), between the spreading lamellas of adjacent drops (e g Cossali et al 2003), or between crowns of droplets splashing in the vicinity of each other (e g Tropea and Roisman, 2000). Several questions arise concerning the resulting influence on mixing preparation prior combustion. At engine start, a liquid film forms which spreads over the surface; crown development and thus secondary

atomization is mainly influenced by local variations of the liquid film induced by drop impact (e g Panão and Moreira, 2005a); re-atomized droplets may emerge from liquid jets induced by pressure fluctuations generated by multiple drop impacts in the liquid film (e g Roisman and Tropea, 2005); interfacial activity in the vicinity of the wall caused by successive injections induce vertical oscillations that may trigger a chain of ejection-and-re-impaction of droplets with a rate faster than the injection frequency (e g . Özdemir and Whitelaw, 1993).

In addition, the fact that a cross flow is present induces drag forces which promote dispersion, partial vaporization and eventual disruption of the droplets before they impact any interposed surface. It has also been suggested, through visualization, that the thickness of the wall-film is decreased by the cross-flow, which makes the size of droplets produced by secondary atomization to decrease (Arcoumanis et al., 1997). The work addressed here follows previous experiments reported in Panão and Moreira (2005b) and is aimed at quantifying the effects of a cross flow on secondary atomization. The flow configuration is that of a gasoline spray impinging onto a flat plate through a cross-flow of air, where shear forces at the interface liquid/gas make the fuel film to develop in a horseshoe shape with an outer rim and dimples inside. The paper includes a detailed characterization of the boundary conditions, so the results will be useful for the validation of numerical models.

2. Experimental setup and Diagnostic techniques

The experimental configuration is described in detail in Panão and Moreira (2005a, b) and only a summary is given here: the spray issues from a commercial pintle-type injector used in PFI gasoline engines with a pintle diameter of 0.79 mm inserted in a cylindrical hole with D = 0.9 mm in diameter. The injector is placed vertically faced downwards at the top of the working section of a wind tunnel (270 mm long, 150 mm wide – Fig. 1) and sprays through a cross stream of air perpendicularly onto the bottom surface, which is located at 50 mm. The sidewalls of the working section are made of glass to provide optical access to the flow and the target surface is made of aluminum with a mean roughness of 2.5 μm.

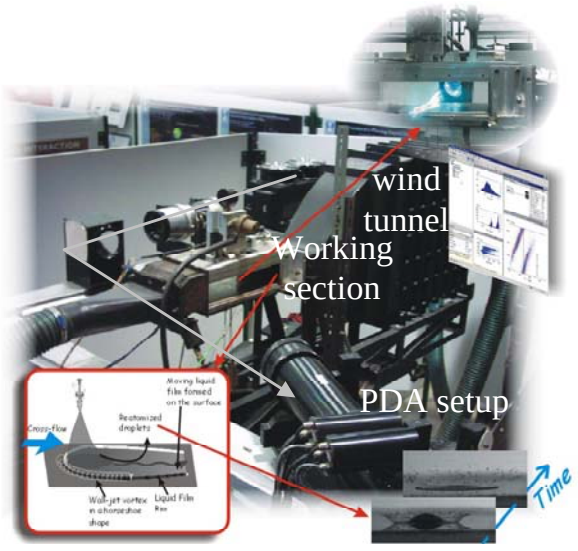

Fig. 1 Experimental setup

The fluid used is commercial gasoline, since there is sufficient evidence to suggest that there are no inert test fluids that can simulate accurately the atomization characteristics of this fuel, e. g., Pitcher and Winklhofer (1998). The properties were measured to be: specific weight, ρ_d = 749.6 kg/m3; viscosity, μ_d = 4.2612×10-4 kg/m/s; refractive index, m = 1.44 and surface tension σ_d = 19.4 mN/m. The injector solenoid is triggered by a TTL pulse controlled by a function generator board, NI5411 from National Instruments, which allows varying the injection frequency, duration and the number of cycles. The injection pressure is manually controlled with a pressure regulation valve. The experiments reported here were obtained with a pressure of injection of 3 bar, a duration and frequency of injection of 10 ms and 10 Hz (aprox. 1200 rpm), respectively, which correspond to a volume rate of 12 litres/h. The cross flow of air was set at a bulk velocity of 5 or 11 m/s with a temperature of 25ºC (± 2ºC).

2.1. Visualization setup

Visualization of the spray/wall interaction is made with a macroscopic Mie scattering system making use of a 9W Argon-Ion laser light source. The beam with a diameter of 2 mm is expanded into a thin sheet (1 mm) with a cylindrical lens and enters the working section from the open end in a plan containing the axis of the injector. The light scattered by the droplets is recorded with a CCD camera (Kodak SR-Series) triggered by the same TTL pulse provided by the injection system to control the aperture of the injector. Recording is made with an image acquisition rate of 1000 Frames per second, a resolution of 256x120 (pixel^2) (which is the maximum resolution provided by the camera) and an exposure time of 0.1 ms.

2.2. Phase-Doppler Anemometer

Local time-resolved measurements of droplet size and velocity are simultaneously obtained with a two-component phase Doppler DANTEC system consisting of a 55X transmitting optics, a 57x10 PDA receiving optics and a 58N10 Covariance processor. More details on the optical characteristics of the system and the main validation parameters can be found in Panão and Moreira (2005b). Measurements are made at 8 mm above the surface. For the flow conditions considered here and for a population of 60000 samples, the number of injection cycles used is usually around 2000. Statistical uncertainties in each size bin were estimated for all ensemble-averages, and were always less than 6% for the mean velocities calculated (Yanta and Smith, 1978) and less than 2% for the mean diameters (Tate, 1982).

3. Results and Discussion

The results presented in this section are threefold. First, Mie scattering and shadowgraph visualization techniques are combined to analyze the macro-scale structures of spray impact under cross-flow. Second, the effects of the cross-flow on the spray dispersion are inferred from comparison of the results obtained for two different cross-flow velocities (5 and 11 m/s) with those obtained for quiescent surroundings (0 m/s). Finally, the third part addresses the effects of the cross-flow on secondary atomization based on spray/wall interaction models reported in the literature for the transition between impact mechanisms and on the experimental characterization of secondary drops.

3.1. Macro-scale structures of spray impact under cross-flow

Mie scattering images are reported in Fig. 2 which shows the influence of a cross-flow on the spray impaction upon a flat surface. Darker areas in the Fig. correspond to a larger concentration of inflowing droplets. The air around the inflowing drops begins to move forward as a result of momentum exchanges and droplets spread out before impact through turbulent dispersion, *i.e.* turbulent exchanges between droplets and air, as shown by Su and Yao (1999). After spray impact, in the absence of cross-flow, the flow structure develops into a wall-jet vortex which forms above the surface and propagates in both the transversal and radial directions (see Fig. 2), generated from momentum exchanges between droplets produced by secondary atomization mechanisms and the surrounding air.

Fig. 2 further shows the transient behavior of the intermittent spray: at 3 ms after start of injection (ASOI), the cone angle of the spray is wider – *leading front of the spray period* - it closes afterwards as seen at 7 ms ASOI – *steady-state spray period* - and slightly opens again (12 ms ASOI), once the injection duration has ended – *spray tail period*. In the presence of a cross-flow, these two macro-scale structures - spray cone angle and wall-jet vortex - are significantly altered: the spray is deflected in the cross-flow direction and both upstream and downstream vortices are suppressed as the cross-flow velocity increases from 5 to 11 m/s.

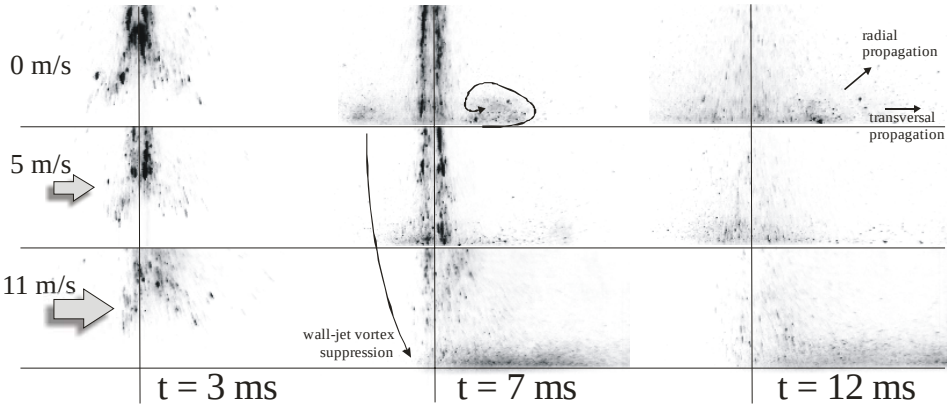

Fig. 2 Effect of the cross-flow on spray deflection and impingement outcome.

Comparing the influence of two cross-flow velocities (5 and 11 m/s) on secondary atomization, it appears that the concentration of secondary droplets above the surface is larger for the highest cross-flow velocity. However, this fact which is associated with the mixing process induced by the cross-flow turbulent structures is better viewed when overlapping Mie scattering and shadowgraph images, as shown in Fig. 3, where the black area corresponds to the liquid phase and the dimples to fuel vapor. Additionally, the measured turbulent boundary layer thickness, [$\delta_{5m/s,}$ $\delta_{11m/s}$], is also depicted (Panão and Moreira, 2005b).

Since the experiment is performed in conditions similar to an engine cold-start, the large volatilization rate of gasoline allows visualizing the transport of vapor by the small scale eddies, as the main mechanism contributing to enhance fuel-air mixing, to provide efficient combustion and smooth engine operation. It is noteworthy that the length scale of the turbulent structures is smaller for 11 m/s as a result of an increasing capacity for mixing, and appears to be confined within the limits of the turbulent boundary layer. Moreover, fuel vaporization appears to be higher for the highest cross-flow velocity used in these experiments, an effect also observed by Choi *et al.* (2004) in experiments performed on a high-pressure swirling spray from a Gasoline Direct-Injection system.

The dark area observed in Fig. 3 above the surface at 7 and 12 ms ASOI, further shows that secondary atomization is enhanced by increasing the velocity of the cross flow. This enhancement can only be caused by more secondary droplets generated by film stripping, or less interaction phenomena between splashing crowns (Cossali *et al.*, 2004), for example, by spreading the impinging droplets over a larger impact area as a result of their deviation by the cross-flow. However, these images can only provide a qualitative picture of the event, and it is the purpose of the following sub-sections to further address these issues with measurements performed by Phase-Doppler Anemometry under two headings: the effect of the cross-flow on spray dispersion; and the effect of the cross-flow on secondary atomization

3.2. Effect of the cross-flow on spray droplets dispersion

The spray droplets dispersion is associated with the interactive motions of droplets and the surrounding environment. The cross-flow influences spray dispersion by: i) promoting secondary break-up of inflowing drops due to imbalance of aerodynamic and surface tension forces; or by ii) promoting momentum exchanges with inflowing droplets and, according to their *responsiveness*, altering their original trajectory and inducing a superposition of trajectories of drops with very different velocity magnitudes in the same region, an event known as 'fan spreading', *e.g.* Hardalupas *et al.* (1989).

In the first case the Weber number defined as $We_{fd} = \rho_f \cdot d_d \cdot |\mathbf{U_d}-\mathbf{V_c}|^2/\sigma_d$, is required to surpass a critical value, where $\mathbf{U_d}$ is the droplet velocity vector (U,V,W) and $\mathbf{V_c}$ the cross-flow velocity vector

$(0,V_c,0)$. However, in the experiments reported here, a maximum of 20% of this critical Weber is attained by the spray droplets.

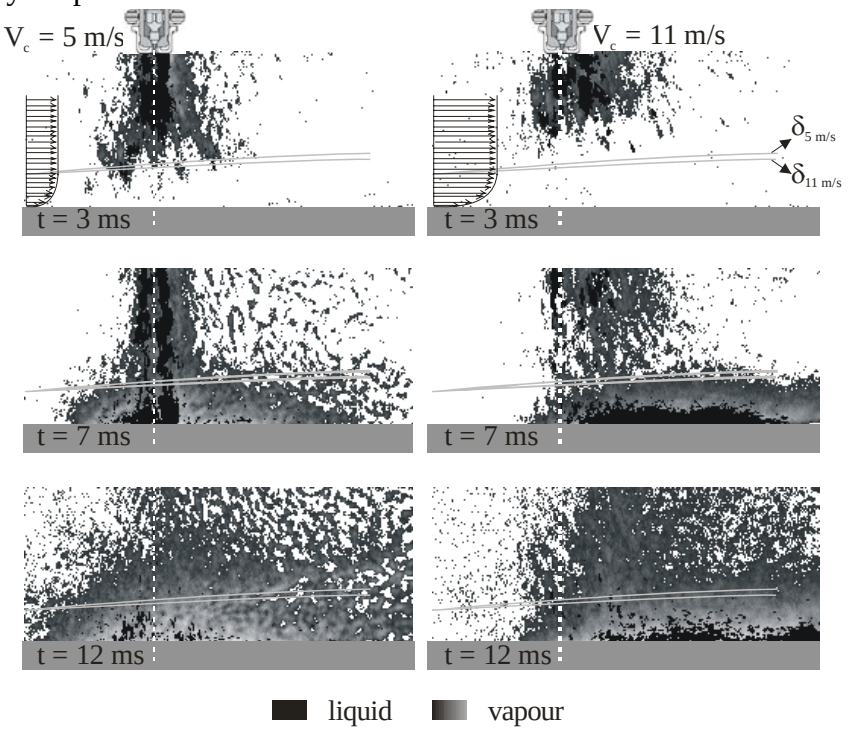

Fig. 3 Combined Mie scattering and shadowgraph images of spray impact for two different cross-flow velocities.

Therefore, the cross flow velocities of 5 and 11 m/s considered in the experiments are not expected to cause any secondary break-ups. This means that the size of inflowing droplets is mainly the result of a balance between pressure and surface tension forces, and then spray dispersion will depend on drag forces exerted by the cross-flow, where 'fan spreading' effects occur. For example, in Panão and Moreira (2005b) 'fan spreading' was found to significantly increase the volume flux of drop sizes up to 50 μm at downstream locations in the cross-flow direction.

Fig. 4 further shows that local values for AMD in the presence of a cross-flow progressively decrease in the downstream direction ($r \rightarrow 12$ mm). And while for $V_c = 5$ m/s, differences in the local AMD values between 33.3D and 38.9D below the nozzle are negligible, with $V_c = 11$ m/s, the AMD increases, which can be attributed to either drop coalescence or 'fan spreading'. Considering that hollow-cone sprays are normally well dispersed, the probability of collision is small and it is not expected to increase in the presence of a cross-flow (Bai *et al.*, 2002). Therefore, it is more likely that 'fan spreading' occurs than drop coalescence, and smaller droplets are actually being removed by the cross-flow before reaching 38.9D below the injector nozzle. Also, the deviation of larger droplets in the cross-flow direction contributes through 'fan spreading' for an increase in the local AMD upstream of the injector central axis (Fig. 4).

Besides, the interaction between the motion of droplets and the turbulent structures of the flow may influence *spray dispersion*. However, the motion of particles in a turbulent flow is rather complex and uneasy to quantify or analyze because it demands simultaneous information on the continuous and dispersed phases. Considering this limitation, an attempt is made to infer on the interaction between the cross-flow and spray dispersion by evaluating its polydispersion degree index (PD_{index}). The PD_{index} is the ratio between a weighted-average to a number-average quantity in the spray: PD_{index} = Sauter Mean Diameter (SMD)/Arithmetic Mean Diameter (AMD).

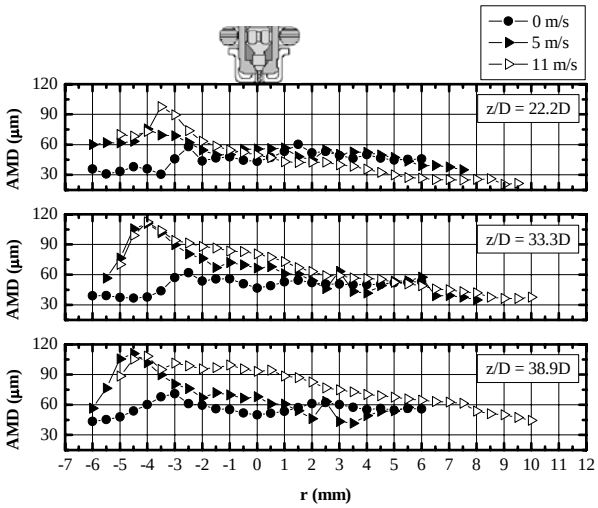

Fig. 4 Arithmetic mean diameter below the injector nozzle at 7 ms ASOI with and without cross-flow at 22.2D, 33.3D and 38.9D, with D = 0.9 mm.

Fig. 5 shows that, while droplet size distribution is not significantly altered along the axial direction for quiescent surroundings, except slight changes in the hollow-cone outer limits, the introduction of a cross flow with an average velocity of 11 m/s leads to a polydispersion degree index $PD_{index} \rightarrow 1$ at almost every measurement location, *i.e.* locally approaching a more uniform drop size distribution. This allows asserting that the size of droplets impacting on the wall in the presence of a cross-flow locally converges to a narrower drop size spectrum in each measurement point. However, a previous work Panão and Moreira (2005b) suggested that this does not produce any significant changes in the size of secondary droplets, which remain rather constant along the radial direction.

3.3. The effect of the cross-flow on secondary atomization

There are three basic issues that sustain the required good boundary conditions in the modeling of spray impingement processes (Bai *et al.*, 2002):

i) appropriate initial conditions of the spray near the injector nozzle;
ii) established criteria for transition between drop impact regimes under certain conditions (dry/wetted surfaces); and
iii) quantitative analysis of the post-impingement drop characteristics.

Here, the main concern is the effect of the cross-flow on secondary atomization. The following discussion is oriented by the aforementioned issues in the order presented above and seeks to provide further insight into our main concern.

3.3.1. Atomization of a port injector

The relatively limited knowledge of the thin liquid sheet break-up mechanisms in port injectors, and the limitation imposed by the width required in the working section of the wind tunnel to accommodate the cross-flow, hinders the measure of the spray characteristics near the injector nozzle, demanding the search for alternative methods of ensuring the availability of appropriate initial conditions. In Grunditz (1996) and Rusche (1997) an empirical procedure has been devised where the information required as inputs are: 1) the probability density function (pdf) of droplet sizes; 2) drop velocity-size correlation and; 3) the average drop mass flux as a function of radius. The advantage of this procedure is that it relies on the information of droplets collected at a downstream plane parallel to the wall, assembled by regions that fall between r and $r+\Delta r$. The third input, average drop mass flux, has not been considered in the present analysis. Fig.s 6 to 8 show the information on the first 2 inputs introduced above for the spray of a port injector. Three cases are considered: i) the spray issuing openly into quiescent surroundings (*free spray*); ii) the spray impacting onto the surface without cross-flow (*spray impact*) and; the spray impingement under a

cross-flow condition (V_c = 11 m/s). The scheme on the right side of Fig. 6 shows the regions of the spray chosen in this analysis. The advantage of providing information on opposite regions, *e.g.* -3 mm ≤ r ≤ 0 and 0 mm ≤ r ≤ 3 mm, is to account for eventual asymmetries in the spray, which means that any interpolation for the remaining area of the spray becomes more accurate.

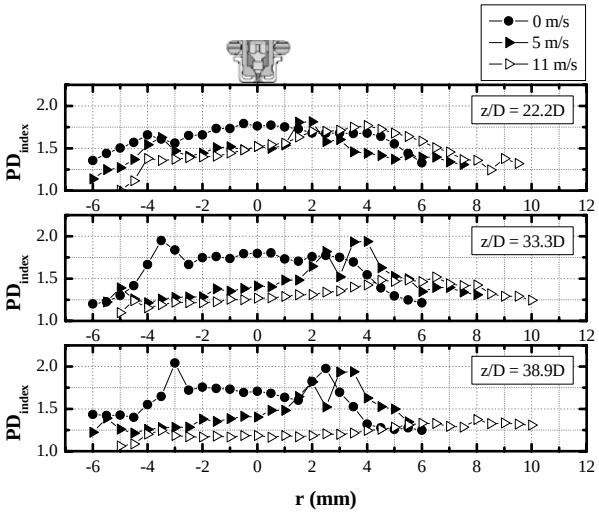

Fig. 5 Polydispersion degree index (PD_{index} = SMD/AMD) below the injector nozzle at 7 ms ASOI, with and without cross-flow for 22.2D, 33.3D and 38.9D, with D = 0.9 mm.

Fig. 6 depicts discrete probability density functions for all cases considered. There are two main observations: i) without cross-flow, and with impact, the size distribution is slightly shifted to the right on the smaller size side from 10 to 20 μm; ii) on the other hand, in the presence of a cross-flow, most droplets of sizes below 80 μm are absent, eventually dragged in its direction shifting the size distribution toward significantly larger diameters.

The results for the 'drop size – axial velocity' correlation (Fig. 7) show larger differences between the free spray and spray impact. Namely a decrease in the axial velocity (an effect attributed to the presence of the wall) in all regions but one, 3 mm ≤ r ≤ 6 mm. By comparison with its opposite region, there is no physical interpretation for this occurrence, except being the result of an asymmetry in the spray. However, between the cases of *free spray* and *spray impact*, the overall deceleration of the mean axial velocity observed on the impinging drops, with no significant changes in their direction (see Fig. 8), clearly shows that the flow is altered once a surface is interposed, and this supports the fact that an accurate modeling of spray impaction requires the knowledge of the flow characteristics near the wall. When the cross-flow is introduced, the deceleration of the axial velocity component due to the wall is still present and a significant increase of the mean radial velocity is measured for every size class. The noteworthy transition between 60 and 75 μm mean axial and radial velocities of impinging drops is not caused by any transition of flow regime, but a consequence of the spray transient behavior. Those droplets with sizes below 60 μm appear later in the spray tail period and have a lower kinetic energy, since the pressure force is now absent because the injector has been closed. This is attenuated further downstream because droplets in this size range, produced during the steady-spray period, have been transported by the cross-flow and, thus, were deviated from their original trajectory. The effects of the wall and cross-flow on the mean axial velocity are particularly important because impact mechanisms, and their transition, dynamically depend on this parameter.

3.3.2. Expected impact regimes of impinging droplets

Most of the research work performed on the impact hydrodynamic mechanisms has been made with single drops, where several phenomena associated with multiple impacts are absent. However, in more recent research works, attention is being given on emerging complexities by multiple impacts

such as: consecutive impacts; interaction between spreading lamellas; crown-crown interaction; interaction between impinging drops and local dynamics of a pre-existing liquid film. But there is still no spray/wall interaction model where all, or a significant part of these complexities are included. This could be considered a limitation for the analysis of spray impingement, relatively to what should be expected from each impact regime in which the impinging droplets fall into. Nevertheless, the quantitative effects of introducing a cross-flow evaluated in the present work recur to single drop impact models, and here, the sorting between impact regimes follows the model presented in Bai *et al.* (2002) based on the Weber (We) and Laplace ($La = \sqrt{\rho_d \sigma_d d_d} / \mu_d$) dimensionless numbers. For a wetted surface: i) $We_c \approx 2 \Rightarrow$ stick→rebound; ii) $We_c \approx 20 \Rightarrow$ rebound→spread; iii) $We_c \approx 1320\ La^{-0.183} \Rightarrow$ spread→splash.

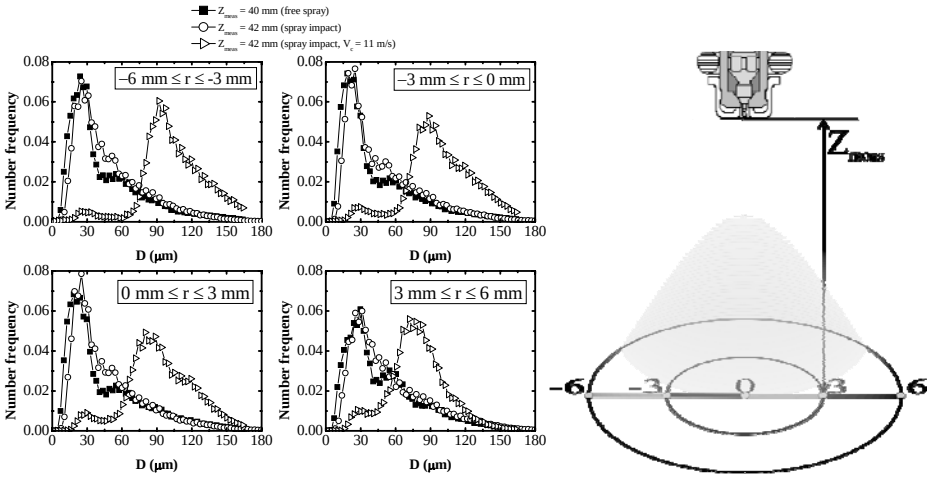

Fig. 6 Drop size distributions at four regions of the spray.

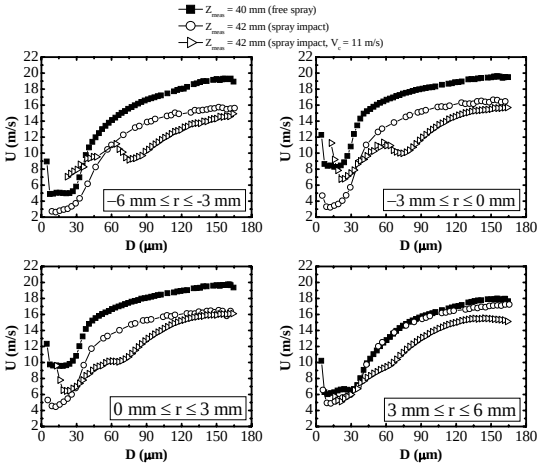

Fig. 7 Drop size-Axial velocity correlation at four regions of the spray.

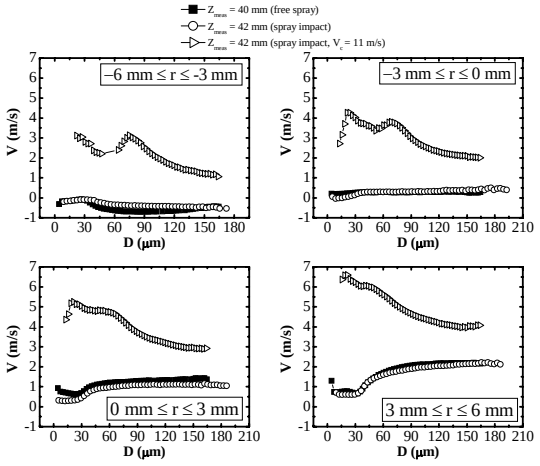

Fig. 8 Drop size- radial velocity correlation at four regions of the spray.

In a previous work (Panão and Moreira, 2005b), the transition between impact regimes described above was used to perform a transient analysis on the effects of the cross-flow on the expected impingement outcome. Here, the analysis is extended and the *overall effects* of the cross-flow are emphasized by using the information collected in all measurement points extrapolated at the wall, and analyzing three outcomes: i) deposition; ii) rebound of droplets and; iii) splash. The last two mechanisms contribute to a secondary atomization of the impinging spray, however, there is a third mechanism, reported by Özdemir and Whitelaw (1993), which is film striping. Unfortunately, this mechanism is not yet considered in current empirical models.

Fig. 9 shows the fraction of droplets expected to stick and spread (m_{dep}) over the surface from

the mass of all validated droplets crossing the PDA control volume (m_{total}). In the absence of cross-flow, the mass deposited on the surface is two orders of magnitude larger than with cross-flow. However, in the presence of a cross-flow, the number of validated drops expected to contribute to the liquid film build-up (N_{dep}), at $r < 6$ mm, is far less than the sample size of drops in the same region without the cross-flow. This means that the cross-flow' dragging of droplets more prone to deposit on the wall, hinders film formation, which is consistent with the visualization reported by Arcoumanis *et al*. (1997), and constitutes an advantage from the engine emissions and performance point of view.

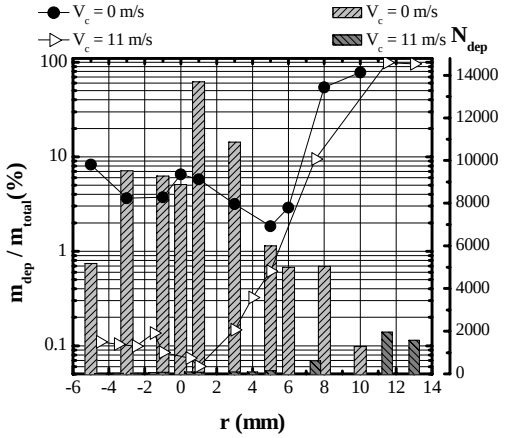

Fig. 9 Fraction from the mass of all droplets that crossed the PDA measurement volume expected to deposit on the wall.

After stick' and spread' contribution to deposition, the impact mechanisms of rebound and splash are at the basis of a secondary atomization. While in quiescent surroundings a significant number of drops were predicted to rebound (Fig. 10), with $V_c = 11$ m/s the minimum sample size required (100 drops/r_i) is never attained, meaning that secondary drops in the presence of cross-flow result from splash or film striping. Fig. 10 further indicates the size of 40 μm as some sort of threshold between those droplets expected to rebound after impact, and those expected to splash. Moreover, while the size distribution of rebound droplets is quite uniform, splashing drops are more polydispersed. This change in the presence of a cross-flow, as observed in Fig. 11, as the number distribution of drops expected to splash approaches uniformity, with less droplets in the ranges of 40-60 μm and 110-160 μm. The dragging exerted on droplets with sizes between 40-60 μm, probably hinders them from ever reaching the wall, which is consistent with the distributions in Fig. 6 where the percentage of these droplets is rather small. An unexpected decrease is also observed in the number of droplets within the size range of 110-160 μm in the case with cross-flow, however, the Weber number ($We_{fd} = \rho_f \cdot d_d \cdot |\mathbf{U_d}-\mathbf{V_c}|^2/\sigma_d$) required for secondary break-up of droplets is only up to 20% of its critical value. Therefore, there are no conditions to expect that break-up mechanisms to occur before these droplets hit the wall. The decrease of the size spectrum of splashing drops diameters implies narrower overall impact energies used to produce secondary droplets, as shown in Fig. 12, although with a negligible influence in the secondary droplets characteristics as shown in the results presented in section 3.3.3.

The discussion up to this point about the effect of the cross-flow on the expected outcome of inflowing droplets can be summarized by the following:

- formation of thinner liquid films;
- narrower size spectrum of droplets, and corresponding dynamic characteristics, expected to produce secondary atomization;

In the following section these effects are used in the analysis of post-impingement drop characteristics.

3.3.3. Analysis of the post-impingement characteristics

The size distributions of secondary drops with/without cross-flow are compared in Fig. 13, and Fig. 14 compares the *overall* data rate, defined as the number of droplets in a size class divided by the total measurement time. There are two clear observations: 1) at 8 mm above the surface (location of PDA measurement plane), the cross-flow removes droplets with sizes below 20 μm from the size distribution and; 2) larger overall data rates imply that more secondary droplets are produced in the presence of cross-flow, quantitatively confirming the observations in the

overlapping Mie-Shadowgraph images depicted in Fig. 3.

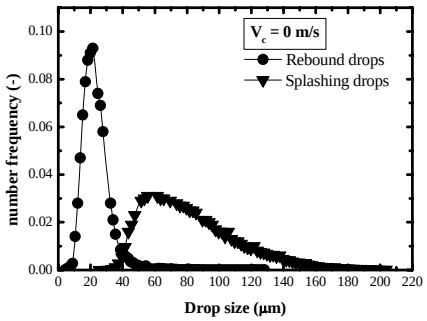

Fig. 10 Size distributions of impinging drops predicted to contribute for secondary atomization (-5 ≤ r ≤ 10 mm).

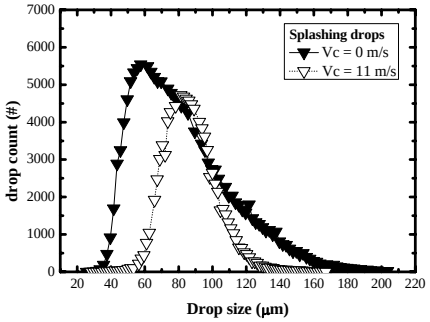

Fig. 11 Size distributions of impinging drops predicted to splash under quiescent surroundings (-5 ≤ r ≤ 10 mm) and in the presence of an 11 m/s cross-flow (-5 ≤ r ≤ 14 mm).

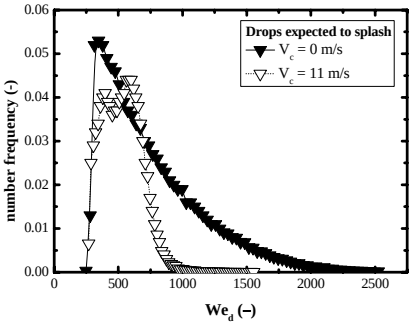

Fig. 12 Discrete probability distributions of the Weber number of drops predicted to splash under quiescent surroundings (-5 ≤ r ≤ 10 mm) and in the presence of an 11 m/s cross-flow (-5 ≤ r ≤ 14 mm).

Thinner liquid films are known to promote splash (Mundo *et al.*, 1998; Cossali *et al.*, 2004; Vander Wal *et al.*, 2006), therefore if the cross-flow inhibits the formation of a thicker liquid film compared to the case without it (also observed by Arcoumanis *et al.*, 1997), then an increase in the production of secondary droplets is obtained through the enhancement of splash. Moreover, it is also likely that stripping of the liquid film by the boundary layer occurs, since the unsteady characteristics of the wave crests are prone to be removed in the form secondary droplets, as described by Özdemir and Whitelaw (1993).

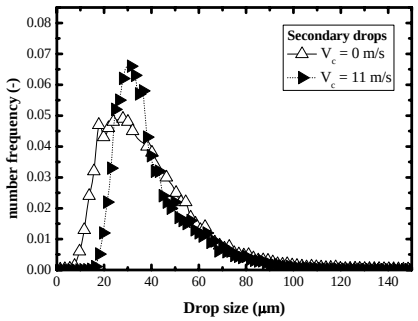

Fig. 13 Size distributions of droplets produced by secondary atomization under quiescent surroundings (-5 ≤ r ≤ 10 mm) and in the presence of an 11 m/s cross-flow (-5 ≤ r ≤ 14 mm).

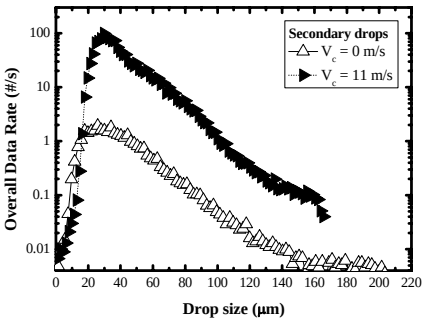

Fig. 14 Overall data rate as a function of drop size of secondary droplets under quiescent surroundings (-5 ≤ r ≤ 10 mm) and in the presence of an 11 m/s cross-flow (-5 ≤ r ≤ 14 mm).

Since a large portion of the kinetic energy of the impinging droplets is used in film stripping to form the interfacial waves, the axial velocity of secondary droplets (U_{sec}) is expected to decrease, as depicted in Fig. 15, and these tend to stay close to the interface, as observed by Özdemir and Whitelaw (1993). However, despite the deceleration observed in the axial velocity of secondary

droplets, momentum exchanges with the cross-flow substantially increase the radial velocity of secondary droplets (V_{sec}). Therefore, the significant changes observed in the direction parameter (γ_{sec}) allow concluding that the transport of droplets by drag forces is, besides thinner films and enhanced production of secondary droplets, one of the main effects of the cross-flow on the secondary atomization, especially to avoid the re-impaction of these droplets, *e.g.* Panão and Moreira (2005a).

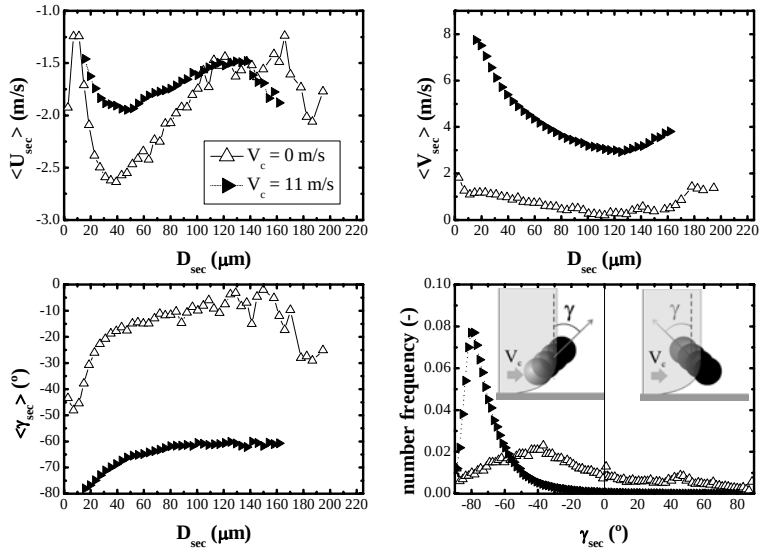

Fig. 15 'Ensemble-average' axial velocity ($<U_{sec}>$), radial velocity ($<V_{sec}>$), direction ($<\gamma_{sec}>$) – drop size correlations, and discrete direction distributions, for secondary droplets under quiescent surroundings ($-5 \le r \le 10$ mm) and in the presence of an 11 m/s cross-flow ($-5 \le r \le 14$ mm).

4. Conclusions

The main features behind the potential of HCCI combustion to reduce emissions and fuel consumption lie in a Controlled Auto-Ignition (CAI), namely the auto-ignition location, the combustion phasing and its duration. A non-symmetric port injection affects the location of auto-ignition, but not the combustion phasing, which requires a strong stratification of the fuel/air mixture. The quality of mixture preparation depends on spray/wall interaction mechanisms which eventually form liquid films on interposed surfaces, especially in conditions similar to engine cold-start. Thus, the secondary atomization as an outcome of spray impact becomes an important feature avoiding that liquid fuel remains in the form of a liquid film over the impact surface.

Moreover, since the most favorable case for HCCI is when the injection event occurs with the intake valve open, interaction between the spray and the airflow is also likely to influence the outcome of impact. However, the availability of information on this phenomenon, with well-defined boundary and operating conditions, similar to those found in a gasoline engine, is one of the major reasons preventing the development of accurate spray/wall interaction models. In this context, the present work is aimed at contributing to provide information for the validation of impingement models, and also deepen the knowledge of the effect of a cross-flow on secondary atomization under conditions similar to cold-start.

The main conclusions can be summarized as follow:

1. the cross-flow decreases the axial velocity of impinging droplets, decreasing the impact energy available for secondary atomization;
2. the dragging of droplets more prone to deposit on the wall leads to the formation of thinner films;
3. with cross-flow, the generation of secondary droplets increases due to
    i. enhanced splash, resulting from thinner liquid films;
    ii. enhanced film stripping by the turbulent boundary layer;
4. transport of secondary droplets by the cross-flow is a major effect and avoids their re-impaction on the wall as observed for quiescent surroundings.

Acknowledgments

The authors also thank Mr. John Laker of Imperial College of Science, Technology and Medicine of the University of London, for his valuable support in designing and building the fuel injection system. The author M. R. O. Panão acknowledges the National Foundation for Science and Technology for providing with financial support through PhD grant SFRH/BD/18669/2004.

References

Arcoumanis C, Whitelaw DS, Whitelaw JH (1997) Gasoline injection against surfaces and films. Atomization and Sprays 7:437-456

Bai C, Rusche H, Gosman AD (2002) Modeling of gasoline spray impingement. Atomization and Sprays 12:1-27

Cao L, Zhao H, Jiang X, Kalian N (2005) Understading the influence of valve timings on controlled autoignition combustion in a four-stroke port fuel injection engine. Proc. IMechE – Part D 219:807-823

Choi J, Lee S, Bae C (2004) Spray and flow-field interaction of gasoline direct injection. Atomization and Sprays 14:159-174

Cossali GE, Marengo M, Santini M (2003) Multiple drop impact on heated surface, 9th Int Conf on Liquid Atom. and Spray Sys., Sorrento, Italy

Cossali GE, Marengo M, Santini M (2004) Impact of single and multiple drop array on a liquid film, In: Proceedings of the 19th Annual Meeting of the Inst. for Liquid Atom. and Spray Sys., Nottingham, UK:493-500

Grunditz D (1996) Model of an impinging gasoline spray. Master's Thesis, University of London, London, UK

Hardalupas Y, Taylor AMKP, Whitelaw JH (1989) Velocity and particle-flux characteristics of turbulent particle-laden jets. Proc. R. Soc. Lond. A 426:31-78

Milovanovic N, Blundell D, Gedge S, Turner J (2005) SI-HCCI-SI Mode transition at different engine operating conditions. SAE Technical Paper 2005-01-0156

Mundo C, Sommerfeld M, Tropea C (1998) On the modeling of liquid sprays impinging on surfaces. Atomization and Sprays 8:625-652

Özdemir IB, Whitelaw JH (1993) Impingement of an unsteady two-phase jet on unheated and heated flat plates. J. Fluid Mech. 252:499-523

Panão MRO, Moreira ALN (2005a) Flow characteristics of spray impingement in PFI injection systems. Experiments in Fluids 39:364-374

Panão MRO, Moreira ALN (2005b) Experimental characterization of an intermittent gasoline spray impinging under cross-flow conditions. Atomization and Sprays 15:201-222

Pitcher G, Winklhofer E (1998) Droplet size and velocity measurements in the spray of a direct injection gasoline injector. In: Proceedings of ILASS – Europe'98

Richter B, Dullenkopf K, Bauer H-J (2005) Investigation of secondary droplet characteristics produced by an isooctane drop chain impact onto a heated piston surface. Experiments in Fluids 39:351-363

Roisman IV, Tropea C (2005) Fluctuating flow in a liquid layer and secondary spray created by an impacting spray. Int J Multiphase Flow 21:179-200

Rusche H (1997) CFD simulation of spray impingement processes, Diploma thesis, University of Hannover, Hannover, Germany

Senda J, Yamada K, Fujimoto H, Miki H (1988) The heat transfer characteristics of a small droplet impinging upon a hot surface. JSME Int J – Series II 31:105-111

Su K, Yao SC (1999) Numerical studies of spray impacting on an infinite plate. Atomization and Sprays 9:431-444

Tate RW (1982) Some problems associated with the accurate representation of droplet size distributions. In: Proceedings of the 2nd International Conference on Liquid Atomization and Spray Systems, Madison, USA

Tropea C, Roisman IV (2000) Modeling of spray impact on solid surfaces. Atomization and Sprays 10:387-408

Vander Wal RL, Berger GM, Mozes SD (2006) Droplets splashing upon films of the same fluid of various depths. Experiments in Fluids 40:33-52

Yanta WJ, Smith RA (1978) Measurements of turbulence-transport quantities with a laser-Doppler velocimeter, AIAA Art. 73-169, 11th Aerospace Science Meeting, Washington, USA

Zhang Y, He B-Q, Xie H, Zhao H (2006) The combustion and emission characteristics of ethanol on a port fuel injection HCCI engine. SAE Technical Paper 2006-01-0631